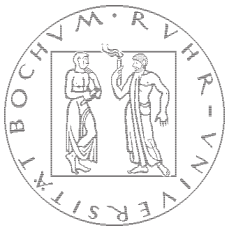

Preprint 01-2006

On the numerical implementation of Variational Arbitrary Lagrangian-Eulerian (VALE) formulations

J. Mosler and M. Ortiz

Ruhr University Bochum
California Institute of Technology

This is a preprint of an article accepted by:

International Journal for Numerical Methods in Engineering (2006)

On the numerical implementation of Variational Arbitrary Lagrangian-Eulerian (VALE) formulations

J. Mosler [*†]

Institute of Mechanics
Ruhr University Bochum
Universitätsstr. 150,D-44780 Bochum, Germany
E-Mail: mosler@tm.bi.ruhr-uni-bochum.de

M. Oritz[*]

Graduate Aeronautical Laboratories
California Institute of Technology
Pasadena, CA 91125, USA
E-Mail: ortiz@aero.caltech.edu

SUMMARY

This paper is concerned with the implementation of variational arbitrary LAGRANGEian EULERian (VALE) formulations, also known as variational r-adaption methods. These methods seek to minimize the energy function with respect to the finite-element mesh over the reference configuration of the body. We propose a solution strategy based on a viscous regularization of the configurational forces. This procedure eliminates the ill-posedness of the problem without changing its solutions, i. e., the minimizers of the regularized problems are also minimizers of the original functional. We also develop strategies for optimizing the triangulation, or mesh connectivity, and for allowing nodes to migrate in and out of the boundary of the domain. Selected numerical examples demonstrate the robustness of the solution procedures and their ability to produce highly anisotropic mesh refinement in regions of high energy density.

1 INTRODUCTION

The stable configurations of a hyperelastic body obey the principle of minimum potential energy. For dynamical and general dissipative materials, the incremental problem can also be recast as a minimization problem by recourse to time discretization [1, 2]. The corresponding finite element approximations then follow from a constrained minimization of the potential energy over the space of interpolants. However, strongly nonlinear problems, e. g., involving finite deformations or unstable material behavior, may lack uniqueness–or even existence–, e. g., as a consequence of buckling or material instabilities. In addition, the space of solutions may not have a natural linear space—much less normed space—structure, and the usual framework of error estimation fails to apply in general. By virtue of this variational structure, the quality of two solutions can be compared simply by comparing their respective energies. Based on this optimality criterion, a class of variational arbitrary EULERian LAGRANGEian (VALE) methods can be formulated. In these approaches, the deformation and the optimal finite-element discretization follow jointly from energy minimization. The resulting energy is the lowest—and, therefore, the attendant solution is the best—among all allowed discretizations, e. g., of a prescribed number of nodes.

[*]DoE through Caltech's ASC/ASAP Center
[†]Deutsche Forschungsgemeinschaft (DFG); contract/grant number: Mo 1389/1-1

The concept of using the underlying variational principle to optimize the discretization enjoys a long tradition dating back, at least, to [3, 4], in the special context of two-dimensional linearized elasticity. By contrast, the connection between mesh optimization and configurational or energetic forces ([5, 6]) has only been recognized recently [7–11]. Braun [7] computed the forces associated with a variation of the nodal positions in the reference configuration in a finite-element discretization and speculated on the possibility of computing such positions so as to attain configurational equilibrium. However, a full solution procedure was not proposed in that work. A variety of solution strategies have recently been proposed based on a steepest gradient algorithm [8]; conjugate gradients [9, 10]; and Newton's method [11, 12]. Thoutireddy and Ortiz, in addition to optimizing the positions of the nodes in the interior and on the boundary, allowed for changes in the connectivity of the mesh. In particular, the connectivity of the mesh was changed during the optimization of the nodal positions so as to maintain a Delaunay triangulation at all times.

Despite the conceptual appeal of variational r-adaption, its robust numerical implementation is not without difficulty. One essential difficulty is that the resulting minimization problem is non-convex and possesses a multitude of local minima. These feature of the extended problem is common in shape and geometry optimization problems. In this work we develop a solution strategy based on a viscous regularization of the configurational forces, i. e., the system of forces conjugate to the location of the nodes in the reference configuration. This viscous regularization is designed to render the minimization problem well-posed while leaving its solutions unchanged. It can equivalently be regarded as the result of replacing the configurational equilibrium problem by a gradient flow. The resulting regularized problem can conveniently be solved by means of NEWTON's method.

As noted previously [9, 10], in addition to optimizing the *geometry* of the mesh, i. e., the location of the nodes in the reference configuration, it is equally important to optimize the *topology*—or connectivity—of the mesh. Indeed, keeping the connectivity of the mesh fixed introduces strong topological—or *locking*—constraints which severely restrict the range of meshes that can be attained and, consequently, the quality of the solution. However, the determination of the energy-minimizing mesh connectivity for a fixed nodal set is a challenging discrete optimization problem. In two-dimensions, an upper bound on the number of different triangulation exists [13] and, consequently, a global minimum is guaranteed. However, the number of different triangulations increases exponentially with the number of nodes [13], and the global minimum cannot be computed in practice. Instead, we propose to modify the mesh topology by applying LAWSON flips [14–16] based on an energy criterion. Specifically, a flip is accepted if it lowers the energy of the solution. The algorithm terminates when all flips raise or leave unchanged the energy of the solution. While this strategy does not guarantee the attainment of the absolute energy-minimizing triangulation, it does identify local minimizers and is found to work reliably in practice.

Most implementations to date constrain the boundary nodes to remain on the boundary. However, this constraint again introduces strong topological obstructions that limit the range of attainable meshes. We overcome this limitation by allowing nodes to migrate in and out of the surface based on an energy criterion. In particular, we allow nodes to move from the boundary to the interior when the move decreases the energy. In order to achieve $O(N)$ complexity, we estimate the energy release associated with the migration of a boundary node to the interior by means of a local problem.

The structure of the paper is as follows. We begin by briefly reviewing the variational framework in § 2. In § 3 we proceed to formulate an extended energy-minimization principle by appending to the equilibrium problem the optimization of the nodal positions and mesh connectivity. In § 4, a Newton solution procedure including a referential viscous regularization

is presented. In § 5 we address the problem of determining energy-minimizing triangulations or mesh connectivities. In § 6 we introduce an algorithm for allowing nodes to migrate in and out of the boundary of the domain. Finally, we close with some concluding remarks in § 7. In addition, examples are included in several sections that illustrate the range and performance of the various solution procedures.

2 THE PRINCIPLE OF MINIMUM POTENTIAL ENERGY

We consider a solid occupying a region $\Omega \in \mathbb{R}^3$ in its reference undeformed configuration. The body deforms under the action of applied body forces and tractions and prescribed displacements. The resulting deformation is described by the deformation mapping $\boldsymbol{\varphi} : \Omega \to \mathbb{R}^3$, which is globally bijective and maps the position $\boldsymbol{X} \in \Omega$ of material particles in the reference configuration to their position $\boldsymbol{x} \in \boldsymbol{\varphi}(\Omega)$ in the deformed configuration. Assuming sufficient differentiability, the local deformation is characterized by the deformation gradient $\boldsymbol{F} := \nabla\boldsymbol{\varphi}$. Throughout this paper we shall be concerned with the equilibrium problem

$$\nabla \cdot \boldsymbol{P} + \boldsymbol{B} = \boldsymbol{0} \qquad \text{in } \Omega, \tag{1a}$$

$$\boldsymbol{\varphi} = \bar{\boldsymbol{\varphi}} \qquad \text{on } \partial\Omega_1, \tag{1b}$$

$$\boldsymbol{P}\boldsymbol{N} = \bar{\boldsymbol{T}} \qquad \text{on } \partial\Omega_2, \tag{1c}$$

where $\partial\Omega_1$ is the displacement boundary; $\partial\Omega_2 := \partial\Omega \backslash \partial\Omega_1$ is the traction boundary; $\bar{\boldsymbol{\varphi}}$ is the prescribed value of the deformation mapping on $\partial\Omega_1$; $\boldsymbol{P}$ is the first PIOLA-KIRCHHOFF stress tensor; $\boldsymbol{B}$ is the body force density; $\boldsymbol{N}$ is the outward unit normal to $\partial\Omega$; and $\bar{\boldsymbol{T}}$ are the applied tractions. We additionally confine attention to hyperelastic materials. Consequently, the stresses follow pointwise as

$$\boldsymbol{P} = \partial_{\boldsymbol{F}} W(\boldsymbol{F}) \tag{2}$$

in terms of the strain-energy density $W(\boldsymbol{F})$. For simplicity, we shall assume $W(\boldsymbol{F})$ to be at least twice continuously differentiable. Equations (1a) and (1c) are the Euler-Lagrange equations of the potential energy

$$I(\boldsymbol{\varphi}) := \int_\Omega W(\nabla\boldsymbol{\varphi}) \, \mathrm{d}V - \int_\Omega \boldsymbol{B} \cdot \boldsymbol{\varphi} \, \mathrm{d}V - \int_{\partial\Omega_2} \bar{\boldsymbol{T}} \cdot \boldsymbol{\varphi} \, \mathrm{d}A \tag{3}$$

We shall be specifically interested in the stable configurations of the solid and we shall assume that such configurations are the minima of the potential energy. This variational characterization of the stable equilibrium points of elastic solids is referred to as the principle of minimum potential energy. We are thus led to the minimum problem

$$\inf_{\boldsymbol{\varphi} \in X} I(\boldsymbol{\varphi}) \tag{4}$$

where X is the configuration space of the solid. Extensive discussions on variational principles in continuum mechanics and their relation to stability may be found in [17].

3 VARIATIONAL r-ADAPTION

Within the preceding variational framework, finite-element approximations may conveniently be characterized as constrained minimizers of the potential energy. While this connection is standard and well-understood, it may stand a brief review in the interest of completeness.

Before a finite element analysis can be performed, the domain of analysis must be defined. We shall assume that the domains of interest are triangulable topological polyhedra [18]. This assumption allows bodies to be described by their boundary, a representational paradigm known as *Boundary Representation of Solids* (B-Rep) in the solid modeling literature [18–21]. A boundary representation consists of: a topological description of the connectivity, incidence and adjacency of the vertices, edges, and faces that constitute the boundary of the body, together with a consistent orientation leading to an unambiguous determination of the interior and exterior of the domain of analysis; and a geometrical description of the surface of the domain. The boundary representation of the domain is particularly important in the present context, since the motion of the nodes in the reference configuration must ensure that the integrity of the boundary representation is preserved.

In addition to the geometrical description of the domain, we consider a *discretization* $(\boldsymbol{X}_h, \mathcal{T}_h)$ consisting of: an abstract simplicial complex $\mathcal{T}_h$, or triangulation (cf, e. g., [18]); and an array of nodal coordinates $\boldsymbol{X}_h := \{\boldsymbol{X}_a,\ a = 1, \dots, n_{\text{node}}\}$. We note that the information encoded by $\mathcal{T}_h$ is strictly topological. The node set is required to contain the vertex set of $\mathcal{T}_h$, but it may be larger than the latter. For instance, for ten-node quadratic tetrahedra the node set contains the mid-side nodes in addition to the vertex nodes. In general the node set will be attached to the cells of $(\boldsymbol{X}_h, \mathcal{T}_h)$, e. g., vertex nodes to vertices, mid-side nodes to edges, and so on. This constraint has the consequence that changes in $\mathcal{T}_h$, e. g., edge swaps, induces changes in $\boldsymbol{X}_h$, e. g., redefinition of mid-side nodes. For every element e in the triangulation the standard isoparametric framework conveniently supplies the local embeddings

$$\boldsymbol{\Psi}_h^e(\boldsymbol{\xi}) = \sum_{a=1}^{n_{\text{node}}^e} \hat{N}_a(\boldsymbol{\xi})\ \boldsymbol{X}_a^e \tag{5}$$

$$\boldsymbol{\psi}_h^e(\boldsymbol{\xi}) = \sum_{a=1}^{n_{\text{node}}^e} \hat{N}_a(\boldsymbol{\xi})\ \boldsymbol{x}_a^e \tag{6}$$

of the standard element domain $\hat{\Omega}$ into $\mathbb{R}^3$. In the above representations $\boldsymbol{\xi}$ are the natural coordinates over $\hat{\Omega}$; $\hat{N}_a$ are the standard shape functions over $\hat{\Omega}$; n_{node}^e is the number of nodes in element e (e. g., $n_{\text{node}}^e = 4$ for simplicial tetrahedral elements and $n_{\text{node}}^e = 10$ for quadratic tetrahedral elements); and $\{\boldsymbol{X}_a^e,\ e = 1, \dots, n_{\text{node}}^e\}$ and $\{\boldsymbol{x}_a^e,\ e = 1, \dots, n_{\text{node}}^e\}$ are the undeformed and deformed nodal coordinates of element e, respectively. The mappings $\boldsymbol{\Psi}_h^e$ and $\boldsymbol{\psi}_h^e$ are required to be diffeomorphisms, i. e., bijective, differentiable, and with differentiable inverse; and $\{\Omega^e = \boldsymbol{\Psi}_h^e(\hat{\Omega}),\ e = 1, \dots, n_{\text{element}}\}$ is required to define a partition of Ω. The deformation mapping for element e then follows as

$$\boldsymbol{\varphi}_h^e = \boldsymbol{\psi}_h^e \circ \boldsymbol{\Psi}_h^{e-1} \equiv \sum_{a=1}^{n_{\text{node}}^e} N_a^e \boldsymbol{x}_a, \tag{7}$$

where

$$N_a^e = \hat{N}_a \circ \boldsymbol{\Psi}_h^{e-1} \tag{8}$$

are the element shape functions over Ω^e. We shall append the usual requirement of conformity, i. e., that $\boldsymbol{\varphi}_h^e$ be the restriction to Ω^e of a continuous mapping $\boldsymbol{\varphi}_h$. This places topological restrictions on the triangulation and constraints on the standard shape functions. By the linearity of the interpolation it follows that

$$\boldsymbol{\varphi}_h = \sum_{a=1}^{n_{\text{node}}} N_a \boldsymbol{x}_a, \tag{9}$$

where N_a are the nodal shape functions over Ω. For the coordinates $\boldsymbol{x}_h$ to be admissible, they must additionally be consistent with the displacement boundary conditions (1b).

By virtue of the preceding representations, the potential energy of the discretized solid follows as

$$I_h(\boldsymbol{x}_h, \boldsymbol{X}_h, \mathcal{T}_h) = I(\boldsymbol{\varphi}_h) \tag{10}$$

Thus, in addition to being a function of deformation I_h is also a function of the discretization of the domain. The principle of minimum potential energy compels us to minimize I_h over its entire domain of definition and thus leads to the discrete minimum problem

$$\inf_{(\boldsymbol{x}_h, \boldsymbol{X}_h, \mathcal{T}_h) \in X_h} I_h(\boldsymbol{x}_h, \boldsymbol{X}_h, \mathcal{T}_h) \tag{11}$$

where X_h is the discrete configuration space of the solid. For ease of reference, we enumerate the constraints that define X_h:

C1 $\mathcal{T}_h$ is a abstract simplicial complex.

C2 The embeddings $\boldsymbol{\Psi}_h^e : \hat{\Omega} \to \mathbb{R}^3$ and $\boldsymbol{\psi}_h^e : \hat{\Omega} \to \mathbb{R}^3$ are diffeomorphic.

C3 $\{\Omega^e = \boldsymbol{\Phi}_h^e(\hat{\Omega}),\ e = 1, \ldots, n_{\text{element}}\}$ defines a partition of Ω.

C4 The discretization is conforming, i. e., $\boldsymbol{\varphi}_h^e = \boldsymbol{\psi}_h^e \circ \boldsymbol{\Psi}_h^{e-1}$ is the restriction to Ω^e of a continuous mapping $\boldsymbol{\varphi}_h$.

C5 The deformations are admissible, i. e., $\boldsymbol{\varphi}_h = \bar{\boldsymbol{\varphi}}$ on $\partial\Omega_1$.

The solution of the minimum problem (11) is not without difficulty. Thus, the constraint C3 that the triangulation span Ω introduces an interplay between discretization and the geometry of the domain; the function $I_h(\boldsymbol{x}_h, \boldsymbol{X}_h, \mathcal{T}_h)$ may be strongly nonconvex in the first two variables; and the minimization of $I_h(\boldsymbol{x}_h, \boldsymbol{X}_h, \mathcal{T}_h)$ with respect to the triangulation is an exceedingly complex discrete minimization problem. The remainder of the paper is devoted to the formulation of solution procedures that effectively address these difficulties.

4 OPTIMIZATION OF THE NODAL COORDINATES

We begin by considering the subproblem of (11) obtained by minimizing $I_h(\boldsymbol{x}_h, \boldsymbol{X}_h, \mathcal{T}_h)$ with respect to $(\boldsymbol{x}_h, \boldsymbol{X}_h)$ while keeping the triangulation $\mathcal{T}_h$ unchanged. In addition, in order to preserve the boundary representation of the domain we begin by enforcing the following constraints:

1. Vertices are fixed points of the reference configuration.
2. Edge nodes are required to remain within their edges.
3. Face nodes are required to remain within their faces.

These constraints introduce boundary conditions in the minimization of $I_h(\boldsymbol{x}_h, \boldsymbol{X}_h, \mathcal{T}_h)$ with respect to $\boldsymbol{X}_h$. In particular, the number of nodes in each surface edge and face remains unchanged. The general minimization problem, including the optimization of the connectivity of the mesh, is considered subsequently in § 5. A more general implementation that relaxes the constraints on the number of surface nodes is presented in § 6.

4.1 Solution strategies based on a NEWTON iteration

Provided that I_h is sufficiently differentiable, whenever $\boldsymbol{x}_h$ and $\boldsymbol{X}_h$ are independent a necessary condition for $(\boldsymbol{x}_h, \boldsymbol{X}_h)$ to be a minimum is

$$\boldsymbol{r}_h := \frac{\partial I_h}{\partial \boldsymbol{x}_h} = \boldsymbol{0} \tag{12a}$$

$$\boldsymbol{R}_h := \frac{\partial I_h}{\partial \boldsymbol{X}_h} = \boldsymbol{0} \tag{12b}$$

On the displacement boundary $\partial\Omega_1$ $\boldsymbol{x}_h$ and $\boldsymbol{X}_h$ are related according to

$$\delta\boldsymbol{x}_h = \frac{\partial\bar{\boldsymbol{\varphi}}}{\partial \boldsymbol{X}_h}\delta\boldsymbol{X}_h. \tag{13}$$

and, hence, are not independent. By virtue of this constraint, at $\partial\Omega_1$ the stationarity condition of the functional I_h with respect to $\boldsymbol{X}_h$ is

$$\frac{\partial I_h}{\partial \boldsymbol{X}_h} + \frac{\partial I_h}{\partial \boldsymbol{x}_h}\frac{\partial\bar{\boldsymbol{\varphi}}}{\partial \boldsymbol{X}_h} = \boldsymbol{0}. \tag{14}$$

instead of (12a) and (12b).

Explicit expressions for the residuals $(\boldsymbol{r}_h, \boldsymbol{R}_h)$ and they linearization have been derived in [9–11]. Based on these expressions, a NEWTON iteration for the solution of the minimum problem (4) may be attempted. However, this iteration fails to converge in general. The essential difficulties are:

1. The minimizers can be vastly non-unique. A case in point is provided by constant strain deformations, in which case the discrete energy I_h is independent of the nodal coordinates $\boldsymbol{X}_h$.

2. The HESSIAN matrix can be singular. By way of illustration, consider the linearized problem near the undeformed configuration. In this case one finds

$$\frac{\partial^2 I_h}{\partial \boldsymbol{X}_h^2} = \frac{\partial^2 I_h}{\partial \boldsymbol{x}_h^2} = -\frac{\partial^2 I_h}{\partial \boldsymbol{x}_h \otimes \partial \boldsymbol{X}_h} = -\frac{\partial^2 I_h}{\partial \boldsymbol{X}_h \otimes \partial \boldsymbol{x}_h} \tag{15}$$

   which is clearly singular. Additional examples of this source of degeneracy are given in Subsection 4.3.

3. The minimization problem is non convex in general. This lack of convexity is illustrated by the examples presented in Subsection 4.3, for which the HESSIAN matrix is found to have a number of negative eigenvalues.

4.2 Viscous regularization of the configurational forces

Askes *et al.* [12] have proposed a dynamic constraint for eliminating the rank-deficiency of the system of equations. The procedure consists of checking if the absolute value of a component of the residual $\boldsymbol{R}_h$ associated with $\boldsymbol{X}_h$ is lower than a numerical tolerance. If so, the corresponding equation is eliminated from the NEWTON step. However, the rank-deficiency of the HESSIAN is not necessarily equal to the number of vanishing components of $\boldsymbol{R}_h$, i. e., the null subspace of the HESSIAN need not coincide with the space spanned by the degrees of freedom

in configurational equilibrium, and the rank-deficiency of the system is not eliminated by constraining the latter space. In addition, the modes corresponding to negative eigenvalues are not stabilized by the procedure.

We propose an alternative stabilization strategy based on a *viscous regularization* of the configurational forces. To this end, we replace problem (11) by the following sequence of problems:

$$\inf_{(\boldsymbol{x}_{n+1},\boldsymbol{X}_{n+1})\in X_h} I_n(\boldsymbol{x}_{n+1},\boldsymbol{X}_{n+1}) \tag{16}$$

where $n = 0, \ldots,$ $(\boldsymbol{x}_0, \boldsymbol{X}_0)$ is given, and

$$I_n(\boldsymbol{x}_{n+1},\boldsymbol{X}_{n+1}) := I_h(\boldsymbol{x}_{n+1},\boldsymbol{X}_{n+1}) + \alpha\,||\boldsymbol{X}_{n+1} - \boldsymbol{X}_n||^2. \tag{17}$$

is a regularized incremental energy function in which $\alpha \geq 0$ is a numerical parameter and $||\cdot||$ is the EUCLIDEAN norm. The function $I_n(\boldsymbol{x}_{n+1},\boldsymbol{X}_{n+1})$ is the potential for the equations resulting from a backward-Euler time discretization of the gradient flow

$$\frac{\partial I_h}{\partial \boldsymbol{x}_h} = \boldsymbol{0} \tag{18a}$$

$$\frac{d\boldsymbol{X}_h}{dt} + \frac{\partial I_h}{\partial \boldsymbol{X}_h} = \boldsymbol{0} \tag{18b}$$

The stationarity conditions are now

$$\frac{\partial I_n}{\partial \boldsymbol{x}_{n+1}} = \boldsymbol{r}_{n+1} = \boldsymbol{0} \tag{19a}$$

$$\frac{\partial I_n}{\partial \boldsymbol{X}_{n+1}} = \boldsymbol{R}_{n+1} + 2\alpha\,(\boldsymbol{X}_{n+1} - \boldsymbol{X}_n) = \boldsymbol{0} \tag{19b}$$

and the corresponding Hessian is

$$\frac{\partial^2 I_n}{\partial \boldsymbol{x}_{n+1}^2} = \left.\frac{\partial^2 I_h}{\partial \boldsymbol{x}_h^2}\right|_{\boldsymbol{x}_{n+1},\boldsymbol{X}_{n+1}} \tag{20a}$$

$$\frac{\partial^2 I_n}{\partial \boldsymbol{x}_{n+1}\otimes\partial \boldsymbol{X}_{n+1}} = \left.\frac{\partial^2 I_h}{\partial \boldsymbol{x}_h\otimes\partial \boldsymbol{X}_h}\right|_{\boldsymbol{x}_{n+1},\boldsymbol{X}_{n+1}} \tag{20b}$$

$$\frac{\partial^2 I_n}{\partial \boldsymbol{X}_{n+1}^2} = \left.\frac{\partial^2 I_h}{\partial \boldsymbol{X}_h^2}\right|_{\boldsymbol{x}_{n+1},\boldsymbol{X}_{n+1}} + 2\,\alpha\boldsymbol{1} \tag{20c}$$

From Equation (20c) it follows that the regularized HESSIAN can be made positive definite by choosing α sufficiently large. In addition, if the iteration converges, it follows that $||\boldsymbol{X}_{n+1} - \boldsymbol{X}_n|| \to 0$. Consequently, the viscous term in (19b) becomes negligibly small as convergence is attained.

In calculations we use a modified NEWTON's iteration including an ARMIJO-type line search strategy and a modified CHOLESKY factorization [22]. In addition, the search directions are checked by an angular criterion [23] in order to verify that they define descent directions. Consequently, the sequence of energies generated by the iterative solution is monotonically decreasing and the solution converges a minimizer of the original problem (11).

The resulting stabilized iterative procedure can be summarized as follows.

1. Initialize $\boldsymbol{x}_h = \boldsymbol{x}_0$, $\boldsymbol{X}_h = \boldsymbol{X}_0$, set $n = 0$.

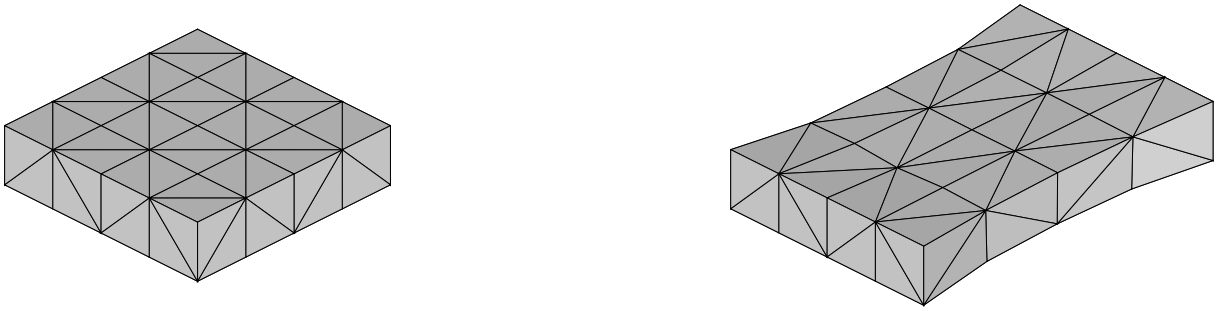

a) b)

Figure 1: Stretching of a neo-Hookean hyperelastic block. Fixed-mesh solution: a) Undeformed configuration; b) deformed configuration.

2. Compute the solution $(\boldsymbol{x}_{n+1}, \boldsymbol{X}_{n+1})$ of the regularized problem (16) by a NEWTON iteration.

3. If $||\boldsymbol{x}_{n+1} - \boldsymbol{x}_n|| < \texttt{TOL}$ and $||\boldsymbol{X}_{n+1} - \boldsymbol{X}_n|| < \texttt{TOL}$ exit.

4. Reset n to $n+1$, go to 2.

Since the iterative procedure produces a monotonically decreasing sequence of energies and, under displacement control, the energy is bounded below, the energy is guaranteed to converge. It should be carefully noted that the choice of α influences the rate of convergence. In particular, a large α tends to slow down convergence. Hence, in calculations we set α to the smallest value resulting in a strictly convex incremental energy function I_n. In particular, we choose α such that the spectrum of $\nabla^2 I_n$ is minorized by a prespecified tolerance TOL. It should be noted that, by this criterion, if the original problem is strictly convex, $\alpha = 0$ and the problem is not regularized.

4.3 Example: Stretching of a slab

Our first example concerns the stretching of a slab of dimensions $L \times L \times L/4$. The slab is clamped on two opposite sides and is subjected to prescribed extensional displacements. The nominal stretch ratio is 1.5 and the entire deformation is applied in one step. The discretization of the domain is coarse and contains 80 elements. In all examples, the material is neo-Hookean with strain-energy density

$$W(\boldsymbol{F}) = \frac{1}{2}\lambda \log^2 J + \frac{1}{2}\mu \left(|\boldsymbol{F}|^2 - 3 - 2\log J \right), \tag{21}$$

In calculations the LAMÉ constants are set to $\lambda = 12115.38$ MN/m^2 and $\mu = 8071.92$MN/m^2, respectively. A similar problem was analyzed in [8] and [12]. However, in contrast to those references we use three-dimensional tetrahedral elements and allow the nodes to move within the boundary.

The undeformed and the computed deformed configuration in the absence of mesh adaption are shown in Figure 1. The energy I_h corresponding to this solution is $I_h^{(1)} = 577.859$ MNm.

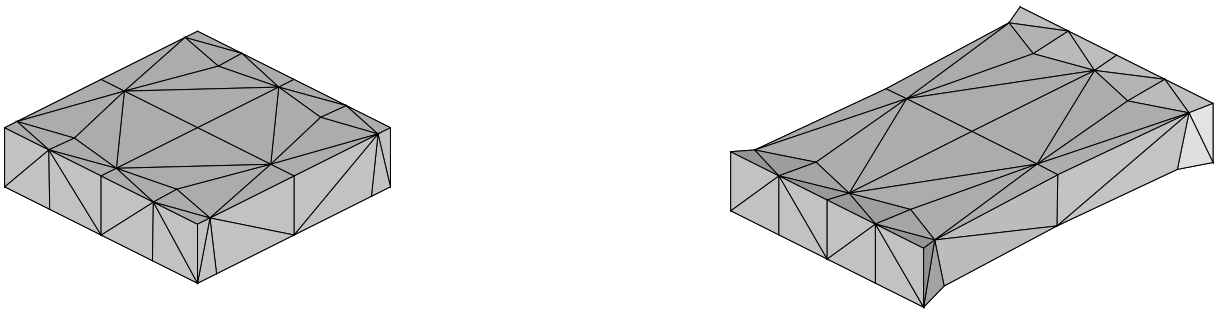

a) b)

Figure 2: Stretching of a neo-Hookean hyperelastic block. r-adapted solution (without mesh-improvement or node migration to and from the surface): a) Undeformed configuration; b) deformed configuration.

By way of comparison, the results obtained by means of the variational r-adaptive scheme are shown in Figure 2. As may be observed in this figure, the nodes move towards the clamped sides. The energy returned by the adaptive scheme is $I_h^{(2)} = 562.300$ MNm, or a 2.8% reduction with respect to the non-adaptive scheme. In order to gage the effect of the motion of the nodes on the boundary we proceed to constrain that motion on two boundary faces. The optimized undeformed and deformed configuration are shown in Figure 3. The resulting energy is now $I_h^{(3)} = 569.678$ MNm, which represents a 1.4% reduction from the non-adaptive energy $I_h^{(1)}$. As expected, $I_h^{(1)} \geq I_h^{(3)} \geq I_h^{(2)}$ and the addition of constraints on the motion of boundary nodes wipes out about half the energy gain due to adaption. This test suggests that the motion of the boundary nodes is important and cannot be neglected in general.

The convexity of the minimization problem and the singularity of the HESSIAN can be monitored by means of the eigenvalues of $\nabla^2 I_h$, Figure 4. The dashed and solid lines in the figure correspond to the converged r-adaptive scheme and a predictor step, respectively. Owing to the large number of null or nearly-null eigenvalues the problem is highly singular. Furthermore, the smallest eigenvalue obtained for the predictor step is $\lambda_{\min} = -5.19745$, which illustrates the lack of convexity of the problem. In consequence, a direct NEWTON's iteration applied to the unregularized problem does not converge in general. However, it should be noted that two-dimensional problems and boundary motion constraints, such as considered by [12], add to the stability of the problem. Under those conditions it is often possible to solve for the r-adapted solution directly without regularization.

5 ENERGY-BASED MESH IMPROVEMENT

Next we turn to the full minimization problem (11), which includes the determination of the energy-minimizing triangulations $\mathcal{T}_h$. Evidently, the triangulation of a node set is not unique, and the discrete energy depends on the precise manner in which the node set is triangulated. Thoutireddy and Ortiz [9, 10] constrained the mesh so as to remain Delaunay at all times, and the Delaunay condition was enforced by means of local Lawson flips [15, 16]. In two dimensions and in the context of potential theory, the Delaunay triangulation does indeed minimize the energy of the body among all possible triangulations [24]. However, in three dimensions

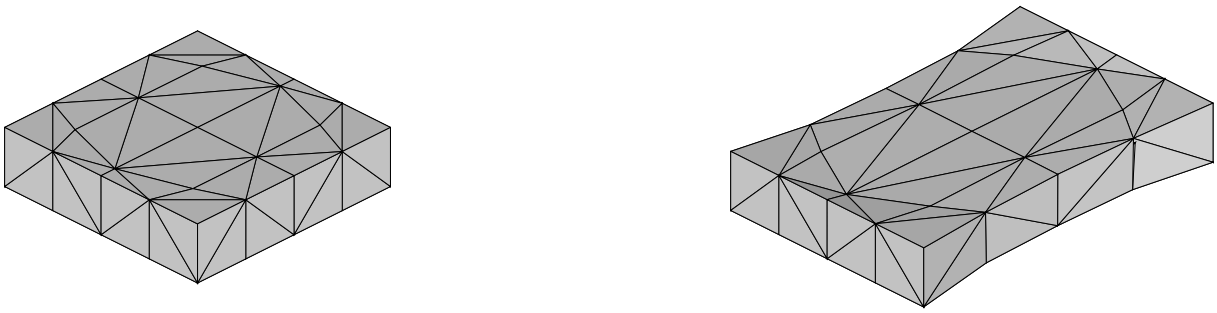

a) b)

Figure 3: Stretching of a neo-Hookean hyperelastic block. r-adapted solution (without mesh-improvement or node migration to and from the surface) with surface nodes constrained on two boundary faces: a) Undeformed configuration; b) deformed configuration.

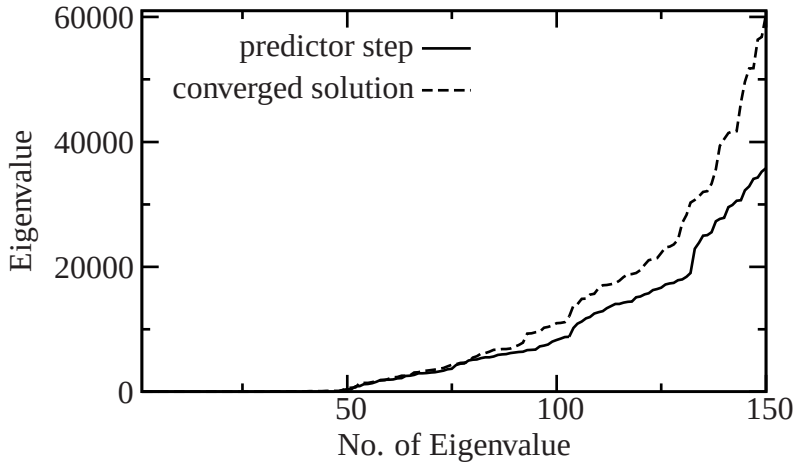

Figure 4: Stretching of a neo-Hookean hyperelastic block. Distribution of the eigenvalues of $\nabla^2 I_h$: a) For a predictor step defined by the standard minimization principle (11); b) for the converged solution

and for general energies the Delaunay triangulation is not necessarily energy-minimizing. In the context of finite elasticity, where the principle of minimum potential is paramount, it is more natural to demand that the mesh connectivity itself, in addition to the mesh geometry, be energy minimizing.

Let $\mathcal{T}_h$ denote a particular triangulation of the node set defined, e. g., by means of a connectivity table. The connectivity table is subject to topological constraints ensuring that the triangulation of the node set define a simplicial complex and the interpolation be conforming. Problem (11) is *discrete* as regards the connectivity optimization and, therefore, its exact solution is generally unattainable for large problems. For instance, for a two-dimensional mesh of N nodes [13] have obtained the lower bound $0.092 \cdot 2.33^N$ on the number of possible triangulations, which is a staggering number for large meshes. Instead of attempting an exhaustive search of the absolute energy-minimizing triangulation, we shall be content to determine triangulations that are local minima of the energy, i. e., triangulations that minimize the energy with respect to a certain class of variations.

According to [25], any triangulation of a two-dimensional node set can be attained by means of a finite sequence of local transformations, or *edge swaps*. These transformations are sometimes called LAWSON flips [14] and consist of swapping the diagonals of the quadrilateral defined by pairs of adjacent triangles. This strategy can be extended to n-dimensional triangulations [14]. However, in general dimensions it is not known whether an arbitrary triangulation can be attained by the application of a finite sequence of local transformations to a given mesh. In three dimensions the local transformations represent all possible triangulations of five noncoplanar vertices of adjacent tetrahedra [14]. These transformations can be classified as T23, T32, T22 and T44 according as to whether Tij transforms i elements into j elements [15, 16].

Suppose that $(\boldsymbol{x}_h, \boldsymbol{X}_h)$ are fixed and let $\mu(\mathcal{T}_h)$ denote the potential energy $I_h(\boldsymbol{x}_h, \boldsymbol{X}_h, \mathcal{T}_h)$ regarded as a function of the connectivity $\mathcal{T}_h$. The objective is to determine the triangulation $\mathcal{T}_h$ that minimizes $\mu(\mathcal{T}_h)$ with respect to all local transformations Tij. To this end, following Joe [26] we begin by listing the faces that are removed by the application of a local transformation. Next, the face list is traversed sequentially and the local optimality of the faces with respect to the function μ is evaluated. Thus, the face is said to be locally optimal if μ is increased by the application of all transformations Tij that remove the face. If a face is μ-locally optimal then no transformation is applied. Otherwise, the best possible local transformation is selected. The algorithm terminates when all faces are locally optimal.

Evidently, by virtue of the energy criterion the application of a local transformation necessarily decreases the energy. However, a locally energy-minimizing mesh is not necessarily globally energy-minimizing, since only local optimality is ensured. Thus, the algorithm just described does not guarantee that a mesh not attainable by local transformations does not decrease the energy further. It should be noted that in applying the preceding algorithm a list of excluded faces that are not to be removed can be specified arbitrarily. In particular, the algorithm can be applied in such a way as to leave the boundary of the body unchanged. It should also be carefully noted that the algorithm applied to minimization problems in general and that it can be applied independently of the r-adaptive procedure described in the foregoing.

Energy-driven mesh-optimization transformations can be built into the r adaption procedure (4.2) simply as follows:

1. Initialize $\boldsymbol{x}_h = \boldsymbol{x}_0$, $\boldsymbol{X}_h = \boldsymbol{X}_0$, $\mathcal{T}_h = \mathcal{T}_0$, set $n = 0$.

2. Compute the solution $(\boldsymbol{x}_{n+1}, \boldsymbol{X}_{n+1}, \mathcal{T}_n)$ of the regularized problem (16) by a NEWTON iteration.

3. Perform energy-minimizing mesh transformations to obtain $(\boldsymbol{x}_{n+1}, \boldsymbol{X}_{n+1}, \mathcal{T}_{n+1})$.

4. If $||\boldsymbol{x}_{n+1} - \boldsymbol{x}_n|| < \texttt{TOL}$, $||\boldsymbol{X}_{n+1} - \boldsymbol{X}_n|| < \texttt{TOL}$ and $\mathcal{T}_n = \mathcal{T}_{n-1}$ exit.

5. Reset n to $n+1$, go to 2.

Again, the iterative procedure produces a monotonically decreasing sequence of energies and since, under displacement control, the energy is bounded below, the energy is guaranteed to converge. Mesh transformations become important and need to be performed in the course of r-adaption. Indeed, the motion of the nodes may lead to mesh entanglement if the transformations are not performed. Conversely, a constant mesh connectivity constitutes a topological constraint that severely limits the meshes that can be attained by r-adaptivity.

5.1 Example: Bending of a notched beam

Our next example concerns the bending of a notched beam of dimensions $101.6 \times 25.4 \times 12.7$ [mm], Figure 5. The length of the notch is 8.47 mm. The beam is clamped at both ends. A vertical displacement is applied to a 3.9 mm region of the top surface centered on the symmetry plane. The material is neo-Hookean hyperelastic with strain-energy density (21). The LAMÉ constants are set to $\lambda = 12115.38$ N/mm^2 and $\mu = 8071.92$N/mm^2, which corresponds to a YOUNG's modulus $E = 21000$ N/mm^2 and a POISSON's ratio $\nu = 0.3$. The energy tolerance for the termination of the iterative solution scheme is set to 1.0×10^{-5}. We exploit the symmetries of the problem to reduce the domain of analysis to one half of the beam. The problem illustrates the behavior of the r-adaption method in the presence of strong singularities such as crack tips and corners.

The deformation of the initial finite element mesh is shown in Figure 5. It contains 392 nodes and 1170 tetrahedral elements (half of the structure). The corresponding energy is $I_h^{(1)} = 75506.8$ MNm.

The solution obtained by means of the r-adaption procedure including energy-based mesh improvements is shown in Figure 6. The energy of the adapted solution is $I_h^{(2)} = 69672.2$ MNm, corresponding to a 8.4% reduction with respect to the fixed-mesh solution. As is evident from the figure, the nodes move towards to regions of highest strain-energy density, namely, the tips of the notches, the region under the center loads, and the corners at the clamped ends. The reconstruction of the mesh in those regions resulting from the energy-based mesh improvements is particularly noteworthy. For instance, a careful examination reveals that the optimal mesh is highly anisotropic in the region of the crack tip. The anisotropy of the mesh stands to reason since the solution near the tip varies slowly along the crack front and rapidly normal to it. That the energy-based criterion should discern this feature of the solution and adapt the mesh to it is quite remarkable.

6 NODE MIGRATION IN AND OUT OF THE BOUNDARY

Throughout the preceding developments we have enforced the constraint that surface nodes remain in the surface and move within their corresponding surface component, namely within their faces or edges; and that vertices in the boundary representation of the domain remain fixed. As a consequence of these constraints, the number of nodes in every edge and face of the boundary remains constant. These boundary conditions introduce topological constraints that limit the range of attainable meshes. A more general and flexible approach that allows nodes to migrate in and out of the boundary is presented next.

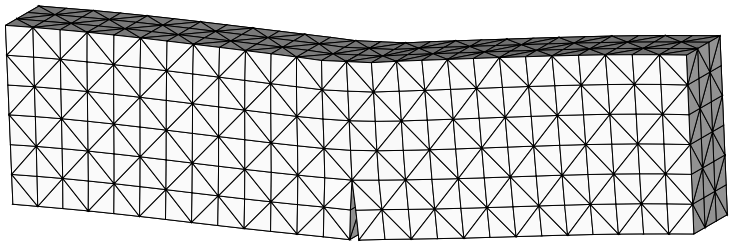

Figure 5: Bending of a neo-Hookean hyperelastic notched beam. Fixed-mesh solution. One-half of the beam is discretized into 392 nodes and 1170 tetrahedral elements

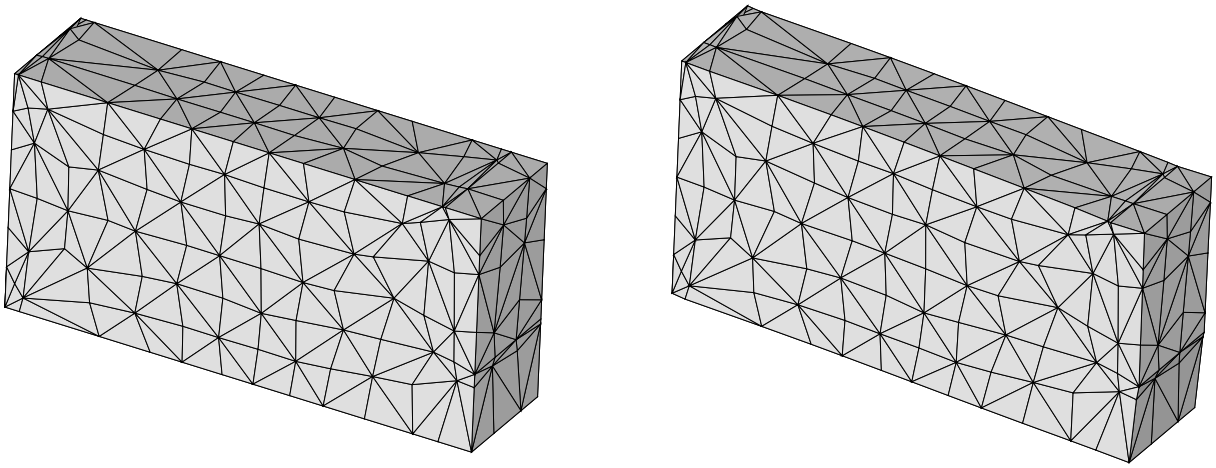

a) a)

Figure 6: Bending of a neo-Hookean hyperelastic notched beam. r-adapted solution with energy-based mesh-improvement (without node migration to and from the surface): a) Un-deformed configuration; b) deformed configuration. The solution is symmetric about the plane of the notch and only one half of the beam is shown in the figures.

Node migration from the interior to the boundary can happen spontaneously during the solution scheme presented in the foregoing and requires no additional algorithmic development. When an interior node collides with the boundary, zero volume elements, or *slivers*, are generated. These slivers are then eliminated during the mesh-improvement phase of the solution.

In order to have a practical $O(N)$ method for allowing nodes to migrate out of the boundary we make two approximations: we localize the problem by considering one boundary node and its ring of adjacent elements in turn; and we estimate the energy release locally by fixing the remaining nodes of the model. Thus, the algorithm is applied by traversing the boundary nodes in turn. For each node that is not a vertex we identify the ring of elements adjacent to the node, or *local neighborhood*. Next we push the node inside its local neighborhood and reconstruct the local mesh. In so doing, care must be exercised in ensuring that all vertices, edges and faces in the boundary representation of the domain be preserved. Based on this new mesh topology, we effect a local optimization consisting of: equilibrating the node, now in the interior; and optimizing its position and the local triangulation. In the course of this local optimization we hold fixed the displacements and positions of all remaining nodes in the model. We then accept the move if the energy release $-\Delta I_{\text{loc}}$ thus estimated is positive and exceeds a prespecified tolerance; and we leave the node unchanged otherwise.

The complete r-adaption procedure accounting for boundary node migration is:

1. Initialize $\boldsymbol{x}_h = \boldsymbol{x}_0$, $\boldsymbol{X}_h = \boldsymbol{X}_0$, $\mathcal{T}_h = \mathcal{T}_0$, set $n = 0$.

2. Compute the solution $(\boldsymbol{x}_{n+1}, \boldsymbol{X}_{n+1}, \mathcal{T}_n)$ of the regularized problem (16) by a NEWTON iteration.

3. Perform energy-minimizing mesh transformations to obtain $(\boldsymbol{x}_{n+1}, \boldsymbol{X}_{n+1}, \mathcal{T}_{n+1})$.

4. Migrate boundary nodes into the interior.

5. If $||\boldsymbol{x}_{n+1} - \boldsymbol{x}_n|| < \texttt{TOL}$, $||\boldsymbol{X}_{n+1} - \boldsymbol{X}_n|| < \texttt{TOL}$, $\mathcal{T}_n = \mathcal{T}_{n-1}$ and no boundary nodes migrate into the interior exit.

6. Reset n to $n + 1$, go to 2.

As in the preceding cases, the iterative procedure produces a monotonically decreasing sequence of energies that, under displacement control, are bounded below and, hence, the energy is guaranteed to converge. We note that the energy release $-\Delta I_{\text{loc}}$ computed from the local procedure is a lower bound on the maximum energy release $-\Delta I_h$ attainable by the migration of the node to the interior. This makes the scheme conservative, i. e., it tends to suppress node migration into the interior. Evidently, better local energy release estimates can be obtained–at some increase in computational complexity–by considering larger local neighborhoods of the boundary nodes including additional rings of elements. The algorithm guarantees that node migration from the boundary indeed lowers the energy of the body. In addition, the migration of each boundary node requires the solution of a local problem involving six degrees of freedom only, and the algorithm is $O(N)$ as desired.

Considerable speed-up may also be achieved in some cases by a simple screening criterion based on the magnitude and direction of the configuration forces. Thus, if a is a surface node located at a point of smoothness of a face in the boundary representation of the domain, $\boldsymbol{N}_a$ is the outward normal at a and $\boldsymbol{R}_a$ is component of $\boldsymbol{R}_h$ at a, then

$$f_a = \boldsymbol{R}_a \cdot \boldsymbol{N}_a \tag{22}$$

a) b)

Figure 7: Bending of a neo-Hookean hyperelastic cantilever beam. Fixed-mesh solution: a) Undeformed configuration; b) deformed configuration.

is the configuration force tending to push the node into the interior. Equivalently, $\boldsymbol{R}_a \cdot \boldsymbol{N}_a$ is the energy-release rate corresponding to an infinitesimal migration of the node into the interior. If a is a non-smooth point of the boundary, the corresponding configurational force is

$$f_a = \max_{\boldsymbol{N}_a \in K_a} \boldsymbol{R}_a \cdot \boldsymbol{N}_a \tag{23}$$

where K_a is the outward normal cone at a. We can then conveniently target surface nodes for possible migration into the interior if f_a exceeds a certain tolerance, and skip over them otherwise.

6.1 Example: Bending of a cantilever beam

Our final example concerns the bending of a cantilever beam of dimensions $L \times L/4 \times L/8$. The tip of the beam is given a deflection of magnitude $L/8$ at two nodes. The material is neo-Hookean hyperelastic with strain-energy density (21). The LAMÉ constants are set to $\lambda = 12115.38$ N/mm^2 and $\mu = 8071.92$N/mm^2, which corresponds to a YOUNG's modulus $E = 21000$ N/mm^2 and a POISSON's ratio $\nu = 0.3$. The energy tolerance for the termination of the iterative solution scheme is set to 1.0×10^{-5}.

The initial discretization contains 54 nodes and 80 tetrahedral elements, Figure 7(a). By way of comparison, the deformation computed without adaption is shown in Figure 7(b). The corresponding energy is $I_h^{(1)} = 57.0510$ MNm.

Next, we recalculate the problem by means of the proposed r-adaption procedure. In the calculation we exercise the energy-based mesh-improvement strategy but do not allow for node migration in and out of the surface. The resulting extended system has 202 degrees of freedom. The computed optimal node location and triangulation are shown in the undeformed and deformed configurations in Figures 8(a) and Figures 8(b), respectively. It is evident from these figures that the nodes move towards the clamped end, i. e., towards the region of highest energy density. The corresponding energy is $I_h^{(2)} = 52.9402$ MNm, i. e., an improvement of about 7.8% with respect to the fixed-mesh solution. In this particular example the initial Delaunay triangulation happens to be locally optimal and no mesh improvement operations need to be performed.

a) b)

Figure 8: Bending of a neo-Hookean hyperelastic cantilever beam. r-adapted solution with energy-based mesh-improvement (without node migration to and from the surface): a) Undeformed configuration; b) deformed configuration.

Finally, we recalculate the problem including r-adaption, energy-based mesh-improvement and node migration in and out of the surface. The surface node that has the greatest inward configurational force is marked by a white circle in Figure 8(a). This node ends up leaving the surface and entering the interior of the domain. The computed optimal node location and triangulation are shown in the undeformed and deformed configurations in Figures 9(a) and Figures 9(b), respectively. The final mesh contains 86 elements. The reconstruction of the mesh in the vicinity of the clamped end is particularly noteworthy. The final energy computed by means of the complete r-adaption procedure is $I_h^{(3)} = 52.2553$ MNm, corresponding to a 9.2% reduction with respect to the fixed-mesh solution.

7 CONCLUSION

In conclusion we emphasize that, for the large deformation problems presented in the foregoing, there is no natural framework for error estimation for several essential reasons: the problems may lack existence or uniqueness; and the space of solutions may lack a natural linear–much less normed–space structure. Under these conditions, the only possible driver for mesh adaption, be it r, h or p, is the variational principle itself. The examples presented in the foregoing illustrate the uncanny ability of energy minimization to generate highly anisotropic mesh refinement in regions of high energy density and non-intuitive mesh patterns. The examples also show that Delaunay triangulation fails to be energy-minimizing in general.

The difficulties and limitations of the approach should also be noted carefully. The mesh adaption problem is highly non-convex and has discrete components, namely, the determination of the optimal triangulation and the partitioning of the nodes between the interior and the boundary. However, as the present work demonstrates these difficulties are far from intractable and can be effectively addressed by means of advanced solution procedures and algorithms. Another clear issue is that r-adaption may add significantly to the solution cost. In particular, the trade off between variational r, h and p adaption are not well understood at present and should be the focus of further research.

a) b)

Figure 9: Bending of a neo-Hookean hyperelastic cantilever beam. r-adapted solution with energy-based mesh-improvement and node migration to and from the surface: a) Undeformed configuration; b) deformed configuration. The surface node marked with a white circle in Fig. 8(a) migrates into the interior of the domain.

ACKNOWLEDGMENT

Support from the DoE through Caltech's ASC/ASAP Center for the Simulation of the Dynamic Response of Solids is gratefully acknowledged. JM is also grateful for support from the Deutsche Forschungsgemeinschaft (DFG) under contract/grant number: Mo 1389/1-1.

References

[1] R. Radovitzky and M. Ortiz. Error estimation and adaptive meshing in strongly nonlinear dynamic problems. *Computer Methods in Applied Mechanics and Engineering*, 172:203–240, 1999.

[2] M. Ortiz and L. Stainier. The variational formulation of viscoplastic constitutive updates. *Computer Methods in Applied Mechanics and Engineering*, 171:419–444, 1999.

[3] G.M. McNeice and P.V. Marcal. Optimization of finite-element grids based on minumum potential-energy. *Journal of Engineering for Industry-Transactions of the ASME*, 95(1):186–190, 1973.

[4] C. Felippa. Numerical experiments in finite element grid optimization by direct energy search. *Appl. Math. Modelling*, 1:93–96, 1976.

[5] J.D. Eshelby. The force on an elastic singularity. *Phil. Trans. R. Soc. Lond. A*, 244:87–112, 1951.

[6] J.D. Eshelby. The elastic energy-momentum tensor. *J. Elasticity*, 5:321–335, 1975.

[7] M. Braun. Configurational forces induced by finite element discretization,. *Proc. Estonian Acad. Sci. Phys. Math.*, 46:24–31, 1997.

[8] R. Mueller and G.A. Maugin. On material forces and finite element discretizations. *Computational Mechanics*, 29:52–60, 2002.

[9] P. Thoutireddy. *Variational Arbitrary Lagrangian-Eulerian method*. PhD thesis, California Institute of Technology, Pasadena, USA, 2003.

[10] P. Thoutireddy and M. Ortiz. A variational r-adaption and shape-optimization method for finite-deformation elasticity. *International Journal for Numerical Methods in Engineering*, 61:1–21, 2004.

[11] E. Kuhl, H. Askes, and P. Steinmann. An ALE formulation based on spatial and material settings of continuum mechanics. Part 1: Generic hyperelastic formulation. *Computer Methods in Applied Mechanics and Engineering*, 193(39-41):4207–4222, 2004.

[12] H. Askes, E. Kuhl, and P. Steinmann. An ALE formulation based on spatial and material settings of continuum mechanics. Part 2: Classification and applications. *Computer Methods in Applied Mechanics and Engineering*, 193(39-41):4223–4245, 2004.

[13] O. Aichholzer, F. Hurtado, and M. Noy. A lower bound on the number of triangulations of planar point sets. *Computational Geometry: Theory and Applications*, 29(2):135–145, 2004.

[14] C.L. Lawson. Properties of n-dimensional triangulations. *Computer Aided Geometric Design*, 3:231–246, 1986.

[15] B. Joe. Three-dimensional triangulations from local transformations. *SIAM J. SCI. COMPUT.*, 10(4):718–741, 1989.

[16] B. Joe. Construction of three-dimensional Delaunay triangulations using local transformations. *Computer Aided Geometric Design*, 8:123–142, 1991.

[17] J.E. Marsden and T.J.R. Hughes. *Mathematical foundation of elasticity*. Dover, New York, 1994.

[18] C. M. Hoffmann. *Geometric and Solid Modeling*. Morgan Kaufmann Publishers, San Mateo, California, 1989.

[19] M. Mantyla. *An Introduction to Solid Modeling*. Computer Science Press, Rockwille, Maryland, 1988.

[20] A. A. G. Requicha. Representations for Rigid Solids: Theory, Methods and Systems. *Computing Surveys*, 12:437–465, 1980.

[21] Radovitzky R. and M. Ortiz. Tetrahedral mesh generation based on node insertion in crystal lattice arrangements and advancing-front-delaunay triangulation. *Computer Methods in Applied Mechanics and Engineering*, 187(3-4):543–569, 2000.

[22] R.B. Schnabel and E. Eskow. A new modified cholesky factorization. *SIAM J. of Scientific Statistical Computing*, 11:1136–1158, 1990.

[23] C. Geiger and C. Kanzow. *Numerische Verfahren zur Lösung unrestringierter Optimierungsaufgaben*. Springer, 1999.

[24] S. Rippa. Minimal roughness property of the delaunay triangulation. *Computer Aided Geometric Design*, 7:489–497, 1990.

[25] C.L. Lawson. Transforming triangulations. *Discrete Math.*, 3:365–372, 1972.

[26] B. Joe. Construction of three-dimensional improved-quality triangulations using local transformations. *SIAM J. SCI. COMPUT.*, 16(6):1292–1307, 1995.